

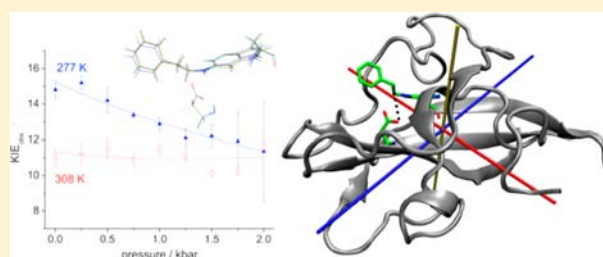
Pressure Effects on Enzyme-Catalyzed Quantum Tunneling Events Arise from Protein-Specific Structural and Dynamic Changes

Sam Hay,^{*,†,‡} Linus O. Johannissen,^{†,§} Parvinder Hothi,^{†,‡} Michael J. Sutcliffe,^{†,§} and Nigel S. Scrutton^{*,†,‡}

[†]Manchester Interdisciplinary Biocentre, [‡]Faculty of Life Sciences, and [§]School of Chemical Engineering and Analytical Sciences, University of Manchester, 131 Princess Street, Manchester M1 7DN, U.K.

S Supporting Information

ABSTRACT: The rate and kinetic isotope effect (KIE) on proton transfer during the aromatic amine dehydrogenase-catalyzed reaction with phenylethylamine shows complex pressure and temperature dependences. We are able to rationalize these effects within an environmentally coupled tunneling model based on constant pressure molecular dynamics (MD) simulations. As pressure appears to act anisotropically on the enzyme, perturbation of the reaction coordinate (donor–acceptor compression) is, in this case, marginal. Therefore, while we have previously demonstrated that pressure and temperature dependences can be used to infer H-tunneling and the involvement of promoting vibrations, these effects should not be used in the absence of atomistic insight, as they can vary greatly for different enzymes. We show that a pressure-dependent KIE is not a definitive hallmark of quantum mechanical H-tunneling during an enzyme-catalyzed reaction and that pressure-independent KIEs cannot be used to exclude tunneling contributions or a role for promoting vibrations in the enzyme-catalyzed reaction. We conclude that coupling of MD calculations with experimental rate and KIE studies is required to provide atomistic understanding of pressure effects in enzyme-catalyzed reactions.



INTRODUCTION

Kinetic isotope effects (KIEs) are a useful probe of reaction mechanism, and inflated intrinsic KIEs remain the definitive hallmark of quantum mechanical hydrogen tunneling in enzymes.^{1–3} The possibilities that tunneling during enzyme-catalyzed reactions may be catalytic and/or can be enhanced by the dynamic coupling of the H-transfer reaction coordinate to the environment—i.e., by promoting vibrations—remains contentious^{4–7} and awaits a definitive experimental test. The observation of strongly temperature-dependent KIEs has been used to infer such environmental coupling,^{8–10} but other experimental probes are needed. One potential probe is hydrostatic pressure. As semiclassical KIEs arise due to differences in vibrational zero-point energy, which have been shown to be insensitive to several kbar changes in pressure (the typical experimental range),^{11,12} the pressure dependence of a KIE has been used as evidence for H-tunneling.^{13–15} We have extended this approach to infer environmental coupling from the combined pressure and temperature (p – T) dependence of H-transfer reactions.^{15–17} While p – T pressure-jump experiments are now established as a useful method of probing the free energy landscape of, e.g., protein folding,¹⁸ the utility of p – T experiments as a probe of tunneling and/or environmental coupling during enzymatic H-transfer remains uncertain as, to date, this approach has only been used to study a small subset of enzymatic reactions—hydride transfers catalyzed by a small number of reductase and dehydrogenase enzymes.^{15,17,19,20} To

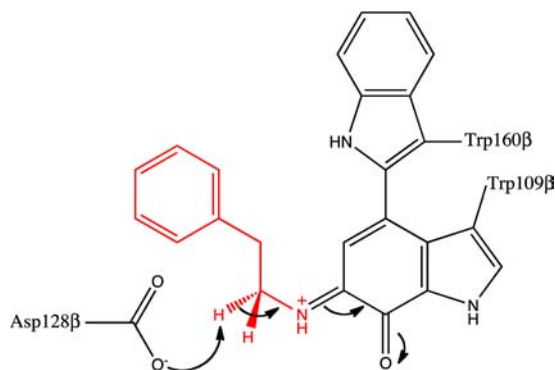
investigate more generally the utility of variable pressure studies in probing such reactions, we have extended the p – T approach here to study an unrelated enzyme reaction, proton transfer during the reductive-half reaction (RHR) of bacterial aromatic amine dehydrogenase (AADH) with phenylethylamine (PEA).

The RHR of AADH involves a rate-limiting proton transfer from a tryptophan tryptophylquinone (TTQ)–substrate iminoquinone adduct to an active-site aspartate (Scheme 1).^{21–23} The RHR with the substrate tryptamine exhibits a H/D KIE of about 55—one of the largest proton KIEs observed in an enzyme²¹—and the proton transfer has a large tunneling component^{21,24} assisted by a putative promoting vibration.^{22,24,25} The RHR with para-substituted PEAs is about 100-fold slower (yet appears to be fully rate-limiting) than with tryptamine, possibly due to a reduction in the reaction driving force.²³ The KIE is also smaller (~10–20) with para-substituted PEAs and, unlike the reaction with tryptamine, is measurably temperature-dependent to varying degrees, depending on the substrate and buffer conditions.²³ In this report, we characterize the p – T dependence of the RHR of AADH with PEA. We show that the origin of the pressure dependence of KIEs can be more complex than previously reported, attributed to anisotropic protein (de)compression mediated by hydrostatic pressure. This has important implications for under-

Received: March 12, 2012

Published: May 26, 2012

Scheme 1. Proposed Mechanism of the Proton-Transfer Step during the RHR of AADH with PEA (The Red Portion Is Derived from the PEA Substrate)



standing H-transfer reactions, which we demonstrate using constant-pressure molecular dynamics (MD) simulations and qualitative modeling with a simple vibronic H-tunneling model.

RESULTS AND DISCUSSION

The pressure dependence of the RHR of AADH with PEA and α - d_2 PEA (dideuterated at $C\alpha$) was measured between 1 bar and 2 kbar (1 bar = 100 kPa = 0.987 atm) at 277, 288, 298, and 308 K (Figure 1 and Figures S1–S4 in the Supporting

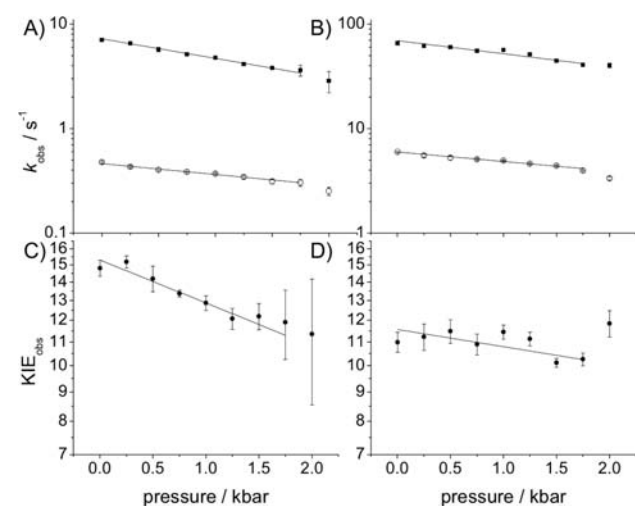


Figure 1. Pressure dependence of the observed rate of the RHR of AADH with 0.5 mM PEA (A,B; filled squares) or 0.5 mM α - d_2 PEA (A,B; open circles) at 277 K (A) or 308 K (B). KIEs observed on this step are shown below in panels C (277 K) and D (308 K). The data from 1 bar to 1.75 kbar are fit to eq 1 while $\Delta\beta^\ddagger$ is fixed to 0. Fitted parameters are given in Table 1 and Table S1.

Information (SI)) using a high-pressure stopped-flow spectrometer. In terms of the biological role of the enzyme, the main interest is the p – T effect around physiological pressure and temperature, but the effects of a broad range of p and T need to be explored to obtain the relevant activation parameters (ΔV^\ddagger , ΔH^\ddagger , etc.). Transient spectral analysis of the RHR (Figure S1) showed no evidence for a change in reaction mechanism or enzyme denaturation—the absorption maxima of the TTQ–PEA adduct at 474 nm formed in the stopped-flow dead-time (~ 10 ms) does not shift with pressure. As the observed spectral changes are similar to those recorded

previously for reduction of AADH by tryptamine,²¹ this finding, coupled with the large KIE observed with para-substituted PEAs, suggests that proton abstraction is fully rate-limiting in stopped-flow measurements with PEAs and is not compromised by kinetic complexity. When the transient data are fit to an exponential function, the fitted amplitudes are pressure-invariant from 1 bar to 1.75 kbar (Figure S1D), suggesting that the enzyme is stable and fully active up to this pressure.

While the observed rate of the RHR, k_{obs} , with PEA decreases with pressure (Figures 1 and S2), the maximal rate is restored upon depressurization, suggesting the effect of pressure up to 1.75 kbar on k_{obs} is reversible. Above 1.75 kbar, the amount of active enzyme significantly decreases (as monitored by the magnitude of the absorbance change during the reaction—an advantage of using pre-steady-state methods for these measurements). This inactivation probably arises due to dissociation of the AADH tetramer into dimers or monomers.²⁶ This process is irreversible, as depressurization does not recover the activity of this fraction of enzyme. The remaining active enzyme does recover upon depressurization, however.

The pressure dependencies of k_{obs} measured at each temperature were fit to eq 1 (Table 1 and Table S1) to

$$k_{\text{obs}}(p, T) = k_0 \exp(-\Delta V^\ddagger(T)p/R_p T) \exp(\Delta\beta^\ddagger(T)p^2/R_p T) \quad (1)$$

$$\text{KIE}_{\text{obs}}(p, T) = \text{KIE}_0 \exp(-\Delta\Delta V^\ddagger(T)p/R_p T) \exp(\Delta\Delta\beta^\ddagger(T)p^2/R_p T)$$

Table 1. p – T Dependence of the KIE^a

T (K)	k_0^{H} (s^{-1})	KIE_0	ΔV^\ddagger ($\text{cm}^3 \text{mol}^{-1}$)	$\Delta\Delta V^\ddagger$ ($\text{cm}^3 \text{mol}^{-1}$)
277	7.2 ± 0.1	15.6 ± 0.3	9.8 ± 0.2	4.2 ± 0.6
288	17.4 ± 0.6	14.2 ± 0.8	7.0 ± 0.9	1.9 ± 1.3
298	39.3 ± 0.7	12.4 ± 0.4	8.2 ± 0.4	0.7 ± 0.7
308	69.5 ± 2.4	11.6 ± 0.4	7.4 ± 0.7	2.0 ± 0.9

^aParameters were determined by fitting the k_{obs} data in Figure 1A and Figure S2 to eq 1 while $\Delta\beta^\ddagger$ is fixed to 0. Additional unrestrained fitted values are given in Table S1. $\Delta\Delta V^\ddagger = \Delta V^{\ddagger\text{H}} - \Delta V^{\ddagger\text{D}}$.

determine the magnitude and temperature dependence of the apparent activation volume (ΔV^\ddagger) and compressibility ($\Delta\beta^\ddagger$).^{14,16} The 2 kbar data points were not used for fitting, and the pressure dependence of the observed KIE can also be fit to eq 1 (Figure S3) in order to guide the eye (we do not use these fitted parameters in our analysis). In all cases, we observed a significant decrease in k_{obs} with pressure as $\Delta V^\ddagger > 0$. There is little curvature observed in Figures 1 and S2, and when fitting to eq 1 we generally find that $|\Delta\beta^\ddagger| < 0$, and there are no obvious trends in the temperature dependence of either $\Delta\beta^\ddagger$ or $\Delta\Delta\beta^\ddagger$ (Table S1). Consequently, we performed the remainder of our analysis by fixing $\Delta\beta^\ddagger = 0$ in eq 1 (Figures 1 and S2). This approach is not unusual¹⁴ and was used in our original study of morphinone reductase (MR).¹⁵

We have postulated that $\Delta\Delta\beta^\ddagger$ may indirectly report on the role of environmental coupling to H-transfer.^{16,17} In an environmentally coupled model of H-tunneling where pressure can perturb both the environmental coupling (promoting vibration frequency) and the H-transfer distance, curvature in $\ln k_{\text{obs}}$ vs p arises when pressure has opposing effects on

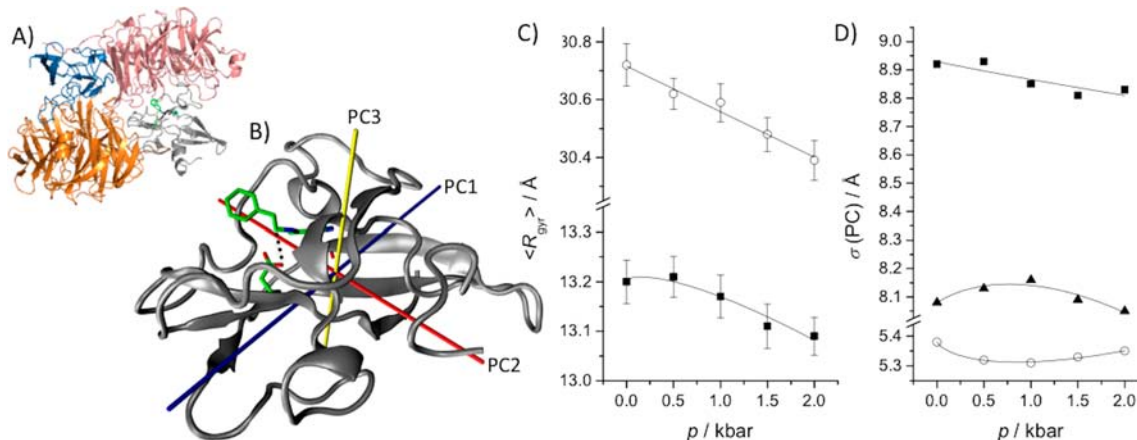


Figure 2. (A) Crystal structure of the PEA-bound AADH tetramer,²³ with the catalytic small subunits shown in blue and gray. (B–D) Effect of pressure on AADH during MD simulations. (B) Orthogonal principal component (PC) vectors for (de)compression (i.e., change in heavy-atom coordinates) of the catalytic (D) subunit from 1 bar to 2 kbar. The vector overlaps between PC1, PC2, PC3, and the C–O vector (dotted black line) are 0.277 ± 0.032 , 0.423 ± 0.012 , and 0.862 ± 0.007 , respectively. (C) Radius of gyration of AADH during the MD simulations. Shown are values for all protein heavy atoms (open circles) and for the catalytic (D) subunit heavy atoms only (filled squares). (D) Deconvolution of $\langle R_{\text{gyr}} \rangle$ for the small subunit into its contributions along the three PC vectors shown in panel B for average structures (filled squares, PC1; filled triangles, PC2; open circles, PC3). Note that $\langle R_{\text{gyr}} \rangle = (\sum_i \sigma(\text{PC}_i)^2)^{1/2}$.

frequency and distance.¹⁶ Consequently, within this framework, the AADH data can be interpreted such that pressure does not perturb *either* the H-transfer distance or the environmental coupling in AADH—one must change, or there would be no change in the KIE with pressure.

At its largest, the magnitude (but not the sign) of $\Delta\Delta V^\ddagger$ on the AADH reaction is similar to that observed in MR¹⁵ (where $\Delta\Delta V^\ddagger = -4.0 \pm 1.3 \text{ cm}^3 \text{ mol}^{-1}$). However, in the case of AADH, $\Delta V^{\ddagger\text{H}}$ (but not $\Delta V^{\ddagger\text{D}}$) is temperature-dependent, so both $\Delta V^{\ddagger\text{H}}$ and $\Delta\Delta V^\ddagger$ decrease with increasing temperature (Table 1)—i.e., the pressure dependence of the KIE decreases with increasing temperature (Figures 1 and S3). These changes in activation volume are not linear with temperature, with the majority of the change in both $\Delta V^{\ddagger\text{H}}$ and $\Delta\Delta V^\ddagger$ occurring between 277 and 288 K. The observed temperature dependence of the KIE, $\Delta\Delta H^\ddagger$, is 6.8 ± 3.9 and $3.8 \pm 3.7 \text{ kJ mol}^{-1}$ at 1 bar and 1.75 kbar, respectively (Figure S4, Table S2)—the relatively large uncertainty in these values is a consequence of having made measurements at only four temperatures. We have not previously observed a significant change in $\Delta\Delta V^\ddagger$ with temperature or a significant change in $\Delta\Delta H^\ddagger$ with pressure. Here, we see a *significant* change in $\Delta\Delta V^\ddagger$ with temperature (Table 1). As $d\Delta\Delta V^\ddagger/dT$ and $d\Delta\Delta H^\ddagger/dp$ are coupled (Figure S5), we posit that in this reaction, $\Delta\Delta H^\ddagger$ is also likely to be pressure-dependent. As mentioned earlier, within the environmentally coupled models of enzymatic H-transfer, the temperature dependence of the KIE is thought to reflect the degree of environmental coupling^{8–10}—i.e., the role of a promoting vibration. The force constant or frequency of an effective promoting vibration is thought to be positively correlated with $\Delta\Delta H^\ddagger$ (discussed later), so a decrease in $\Delta\Delta H^\ddagger$ with pressure could be interpreted as reflecting a decrease in promoting vibration frequency with increasing pressure.

In cases where both the observed rate and KIE decrease, one must also consider the potential effects of kinetic complexity. In AADH, proton abstraction is preceded by formation and dehydration of a carbinolamine intermediate to generate an enzyme–substrate iminoquinone intermediate from which proton abstraction takes place.²¹ Under steady-state conditions, a definitive test for kinetic complexity would require measure-

ment of KIEs with tritiated substrate. This is not possible from a practical viewpoint using rapid mixing stopped-flow methods. However, the spectral analysis described earlier suggests that carbinolamine formation and dehydration occur in the dead time of the stopped flow at all pressures investigated and that proton transfer is still likely fully rate-limiting at high pressure.

Unlike in AADH, the effect of pressure on the old yellow enzymes (OYEs) MR¹⁵ and pentaerythritol tetranitrate reductase (PETNR)¹⁷ is to increase the observed rate of H-transfer. We have interpreted this effect as arising due to a compression of the active site that narrows the activation barrier^{15–17,27,28}—i.e., what we loosely call barrier compression. Can the decrease in k_{obs} with pressure observed in AADH then be explained by barrier decompression? To investigate whether pressure causes active-site (de)compression in AADH, constant-pressure MD simulations of the PEA–iminoquinone intermediate of the AADH tetramer were performed at 500 bar intervals between 1 bar and 2 kbar at 298 K (Figures 2 and S6). Not surprisingly, pressure causes a significant reduction in the average radius of gyration, $\langle R_{\text{gyr}} \rangle$, of both the complete AADH tetramer and the catalytic subunit (like previous studies,^{21,22} all analysis presented is on the D chain). It therefore seems reasonable to expect that increasing pressure might compress the active site, and hence the donor–acceptor (D–A) distance, as in the case of MR.^{27,29} However, the average structures of the TTQ–PEA adduct from the MD simulations do not differ significantly between 1 bar and 2 kbar (Figure 3A). Additionally, the heavy-atom (C–O) and H–O distance trajectories, binned and fitted to Gaussian distributions, reveal no significant change in either distance with pressure (Figure 3B).

To understand why overall compression of the enzyme might not translate into D–A compression, we carried out principle components analysis (PCA) on the absolute change in atomic coordinates of the small subunit between 1 bar and 2 kbar, identifying three orthogonal vectors of (de)compression shown in Figure 2B. The change in $\langle R_{\text{gyr}} \rangle$ was deconvoluted along these three vectors (Figure 2C,D). The effect of pressure is quite anisotropic, with the majority of the change in $\langle R_{\text{gyr}} \rangle$ with pressure occurring in one dimension. The heavy-atom (C–O) vector, which approximately represents the H-transfer reaction

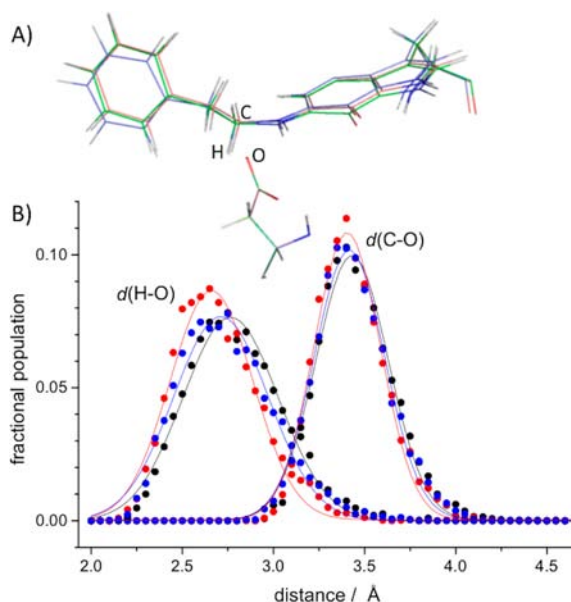


Figure 3. (A) Catalytic subunit TTQ-PEA iminoquinone adduct (Trp-160 β moiety not shown) structures averaged over 7 ns of MD trajectory at 1 bar (green), 1 kbar (orange), and 2 kbar (blue). Structures are each aligned over all heavy atoms of the aspartate, and the donor C, acceptor O, and transferred H are labeled. (B) C-O and H-O distance trajectories at 1 bar (black), 1 kbar (red), and 2 kbar (blue) binned every 0.05 Å and fit to a Gaussian function. The fitted parameters are given in Table S4.

coordinate, is aligned at an average angle of $74^\circ \pm 9^\circ$, $65^\circ \pm 2^\circ$, and $30.5^\circ \pm 0.2^\circ$ to the three principal component vectors, respectively. Consequently, the reaction coordinate is most closely aligned to the coordinate (PC3) with the least (de)compression. Together, these data suggest that 2 kbar of pressure behaves anisotropically on AADH by reducing the radius of gyration but not significantly altering the D-A distance or orientation.

Spectral density analysis^{30–33} of the AADH-tryptamine iminoquinone complex from MD simulations has previously identified a putative promoting vibration at $\sim 165\text{ cm}^{-1}$ that transiently compresses the reaction coordinate.²² Here, we performed analogous calculations on the AADH-PEA catalytic subunit at 1 bar, 1 kbar, and 2 kbar (Figures 4 and S7). Modes that most strongly contribute to D-A compression lie in the low-frequency region, as $J(\omega) \propto A\omega^2$, where A is the amplitude of compression, ω the angular frequency, and $J(\omega)$ the amplitude of the spectral density. Figure 4 is dominated by a prominent peak at $\sim 120\text{ cm}^{-1}$ and a number of peaks around 250 cm^{-1} . Increasing pressure appears to increase the population of the $\sim 120\text{ cm}^{-1}$ mode and concomitantly decrease that of the $\sim 250\text{ cm}^{-1}$ mode, which will decrease the apparent frequency of the effective promoting vibrations. If the reaction is described using a simple vibronic H-tunneling model,^{16,34–38} then this will lead to decreases in both the magnitude and temperature dependence ($\Delta\Delta H^\ddagger$) of the KIE with increasing pressure (Figures 5 and S9).

To further investigate the effect of pressure on these modes, we employed frequency deconvolution by digital filtering,²² where motion outside a specified frequency range is zeroed (Figure S8). The overall (unfiltered) motion shows poor correlation between either the C (donor) or O (acceptor) motion and the C-O distance. However, this correlation

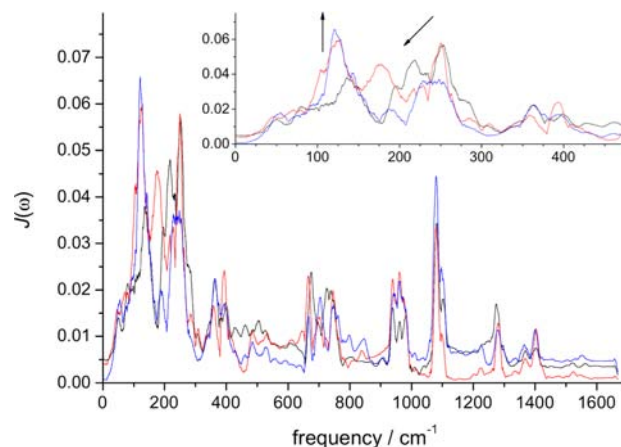


Figure 4. Spectral density analysis of the small subunit C-O velocity spectral density at 1 bar (black), 1 kbar (red), and 2 kbar (blue). The inset shows how pressure decreases the effective frequency by increasing the amplitude of the $\sim 120\text{ cm}^{-1}$ peak while concomitantly down-shifting the $\sim 250\text{ cm}^{-1}$ peak(s). Additional spectral densities showing the motion of C and O projected onto the C-O vector are shown in Figure S7.

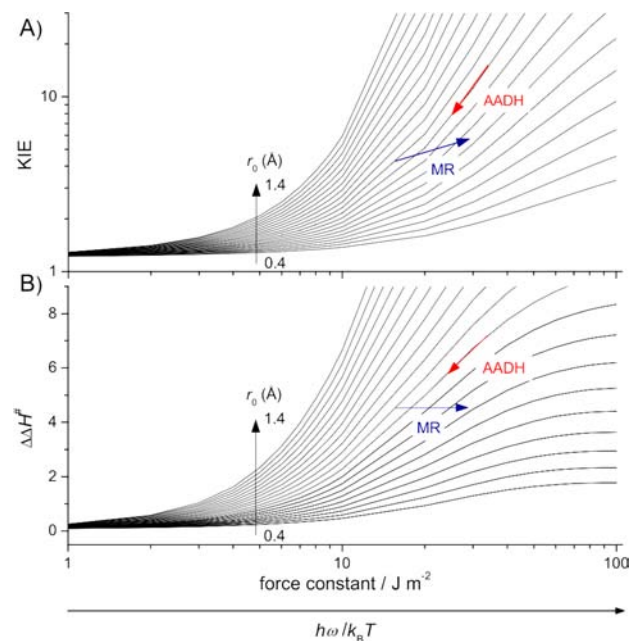


Figure 5. Numerical modeling of the promoting motion force constant dependence of the magnitude (A) and temperature dependence (B) of a non-adiabatic KIE for various equilibrium H-transfer (r_0) distances. KIE and $\Delta\Delta H^\ddagger$ values were calculated using a modified^{24,38} Kuznetsov and Ulstrup vibronic model,³⁵ where the wave function of the transferred H is modeled using Morse potentials, using the same parameters as used previously for the AADH-tryptamine reaction.²⁸ The red and blue arrows show *qualitatively* how pressure is proposed to modulate the KIE on the AADH and MR reactions by lowering the effective force constant in AADH at constant r_0 , and by decreasing r_0 while concomitantly increasing the force constant in MR.^{15,16}

improves when only the $25\text{--}300\text{ cm}^{-1}$ region, which encompasses the peaks of interest (Figure 4), is examined (Table 2). Further deconvolution shows that the C motion is most strongly correlated with the C-O distance between 25 and 175 cm^{-1} , while the O motion is only strongly correlated between 175 and 300 cm^{-1} (Table S5). This is consistent with

Table 2. Frequency Deconvolution by Digital Filtering^a

	R^2 for C/O		
	unfiltered	25–300 cm^{-1}	25–1700 cm^{-1}
1 bar	0.38/0.30	0.61/0.45	0.62/0.45
1 kbar	0.17/0.38	0.69/0.36	0.67/0.38
2 kbar	0.39/0.40	0.60/0.42	0.61/0.41

^a R^2 value is the squared absolute correlation coefficient between the donor C or acceptor O PC1 and the C–O distance for each frequency range. Additional values are given in Table S5.

the spectral densities shown in Figure S7, which reveal that the $\sim 250 \text{ cm}^{-1}$ peaks correspond primarily to motion of O.

The variance of the unfiltered C–O distance—a measure of the D–A distance sampling—decreases with increasing pressure; however, this includes motion that is not symmetrically coupled to the H-coordinate (as is evident from the low R^2 values). The data filtered between 25 and 300 cm^{-1} (and 25–1700 cm^{-1}) show the opposite trend (Table S5), with a significant (13%) increase from 1 bar to 1 kbar, and essentially no change from 1 kbar to 2 kbar (2% decrease). As the magnitude of the KIE is generally assumed to be dominated by the H-transfer distance, then greater distance sampling will lead to shorter H-transfer distances,^{35,36,39} and thus the KIE will decrease with pressure, principally from 1 bar to 1 kbar—as is observed in Figure 1.

This increased degree of D–A distance sampling with pressure can also, at least qualitatively, independently explain the difference in the pressure dependence of the KIE ($\Delta\Delta V^\ddagger$) between the AADH-catalyzed H-transfer and hydride transfer in the MR-catalyzed reaction with NADH. The MR KIE increases with pressure, yet $\Delta\Delta H^\ddagger$ is not measurably pressure-dependent,¹⁵ as pressure is thought to both increase the frequency of the effective promoting vibration and compress the average D–A distance (these two phenomena are expected to alter the magnitude of the KIE and $\Delta\Delta H^\ddagger$ in opposing directions).¹⁶ Figure 5 illustrates the change in KIE with the promoting vibration force constant for a range of average D–A distances. For AADH, the slope of the curves will qualitatively correspond to $\Delta\Delta V^\ddagger$, since the effect of pressure is predominantly on the promoting vibration frequency, ω . Increasing temperature (decreasing $\hbar\omega/k_B T$) will shift the system along this curve, decreasing both the KIE and the slope, and hence $\Delta\Delta V^\ddagger$. For MR, an increase in pressure means moving between different curves (changing r_0) in the direction shown, so that the resulting pressure dependence curve has a smaller slope, consistent with the observation of a temperature-invariant $\Delta\Delta V^\ddagger$ in MR.¹⁵

The data in Figures 2 and 3 suggest that pressure does not significantly perturb the active-site geometry in AADH. What then is the origin of the change in effective frequency with pressure? As pressure is thought to act by perturbing existing equilibria,^{14,18,26} the data in Figure 4 could be interpreted such that the reactant state is in two rapidly (sub-nanosecond time scale) interconverting states, each with a slightly different compressive mode. At atmospheric pressure, the 250 cm^{-1} “state” is slightly favored, and as the pressure is increased the 120 cm^{-1} state becomes more favored. This would arise if the atomic volume of AADH in the 120 cm^{-1} state is smaller than in the 250 cm^{-1} state. As the equilibrium constant must be near unity (both states are visible at all pressures), the difference in volume, and thus geometry, could be quite small ($<10 \text{ cm}^3 \text{ mol}^{-1}$). If this is the case, the reaction barriers (and associated

KIEs) may differ between these two states, and the temperature dependence of the KIE could arise from the mixing of these two states—a recently proposed two-(reactant) state model has been proposed to be able to account for temperature-dependent KIEs (as opposed to promoting vibrations).⁶ Ultimately, the origin of p – T dependence of the AADH reaction is probably complex. In any case, it appears that our earlier assumptions that pressure will generally compress an enzyme active site and decrease the D–A separation^{15,17,27} are oversimplistic.

CONCLUDING REMARKS

In summary, we have shown that detailed understanding of pressure-dependent effects on KIEs requires atomistic understanding through the coupling of MD calculations and experimental studies of reactions rates. Without this atomistic insight, studies of pressure effects are limited as probes of either tunneling or coupling to protein dynamics. In contrast to our studies with MR,^{27,29} pressure behaves anisotropically on AADH, and the active site does not appear to be measurably compressed along the reaction coordinate at 2 kbar (at least at 298 K). While pressure does not significantly modulate the D–A distance in AADH, it does appear to decrease the effective frequency of the promoting modes that transiently compress the D–A distance, and thus probably facilitates the H-transfer reaction. This contrasts with other reported p – T studies of H-transfer reactions,^{15,17} where compression appears to directly modulate both the D–A distance and the frequency of the apparent promoting vibration. Finally, and perhaps most importantly, we have now demonstrated that pressure-dependent KIEs are not a definitive hallmark of quantum mechanical H-tunneling. More specifically, while semiclassical KIEs are still expected to be pressure-independent, KIEs on enzymatic H-tunneling reactions appear to be variably pressure-dependent, and a pressure-independent KIE should not be used to exclude a tunneling contribution or a role for promoting vibrations.

EXPERIMENTAL SECTION

All reagents were purchased from Sigma Aldrich (St. Louis, MO). α - d_2 -PEA was synthesized as described previously.²³ AADH was isolated from *Alcaligenes faecalis* IFO 14479, purified as described previously⁴⁰ and reoxidized, as described previously,²³ immediately prior to use. High-pressure rapid reaction kinetic experiments were performed using a Hi-Tech Scientific HPSF-56 high-pressure stopped-flow spectrophotometer (TgK Scientific, Bradford on Avon, UK). Measurements were typically performed with 3 μM AADH and 0.5 mM PEA or α - d_2 -PEA (post-mixing concentrations; the saturation constant for PEA is $<5 \mu\text{M}$ ²³) in 10 mM Tris, pH 8.0. The RHR was monitored by following the reduction of the TTQ cofactor (474 nm absorption; Figure S1 in the SI), and data were analyzed by fitting to a single or double (to include a minor slow component) exponential function. Typically 3–5 measurements were made under each condition, and the average ± 1 standard deviation is presented.

MD simulations and spectral density calculations were performed essentially as described previously.^{22,29} Briefly, constant temperature and pressure (CPT) simulations with the Nosé–Hoover thermostat were run using CHARMM32⁴¹ with the CHARMM22 force field,⁴² with 3 ns of equilibration at 1 bar prior to additional pressurization with 250 bar every 100 ps. MD simulation for analysis was then performed for a further 7 ns. Spectral densities were calculated for a 3 ns window, starting 1 ns after initial equilibration for 1 bar and 3 ns after pressurization for 1 and 2 kbar. Spectral densities were calculated for the vector for motion of the donor carbon (ν_C) and the vector for motion of the donor carbon projected onto the C–O unit vector ($\nu_{C/C-O}$). Spectral density for a vector ν is the Fourier transform of the

autocorrelation function of v .⁴³ Digital filtering was performed as described previously.²²

■ ASSOCIATED CONTENT

■ Supporting Information

Additional experimental data and simulation/modeling analyses; representative stopped-flow data (Figure S1); pressure dependence of rate constants (Figure S2) and KIE values (Figure S3); Eyring plots for rates of H-transfer (Figure S4); correlation plots for $d\Delta\Delta V^\ddagger/dT$ and $d\Delta\Delta H^\ddagger/dp$ for an idealized reaction where $\ln \text{KIE}$ vs p and $\ln \text{KIE}$ vs $1/T$ are linear; representative MD trajectories (Figure S6); AADH velocity spectral densities (Figure S7); plots of $d(\text{C1}-\text{O2})$ vs C1 and O2 motion for unfiltered and specified frequency ranges (Figure S8); numerical modeling of promoting motion force constant dependence of the magnitude and temperature of a non-adiabatic KIE for various equilibrium D–A values (Figure S9); tabulated kinetic parameters derived from stopped-flow kinetic data (Table S1); tabulated Eyring parameters vs pressure (Table S2); tabulated computational parameters from simulation data (Tables S3, S4); additional references and complete refs 41 and 42. This material is available free of charge via the Internet at <http://pubs.acs.org>.

■ AUTHOR INFORMATION

Corresponding Author

sam.hay@manchester.ac.uk; nigel.scrutton@manchester.ac.uk

Notes

The authors declare no competing financial interest.

■ ACKNOWLEDGMENTS

This work was funded by the UK Biotechnology and Biological Sciences Research Council (BBSRC). S.H. is a BBSRC David Phillips Fellow. N.S.S. is a Royal Society Wolfson Merit Award holder and an Engineering and Physical Sciences (EPSRC) Established Career Fellow.

■ REFERENCES

- (1) Cha, Y.; Murray, C. J.; Klinman, J. P. *Science* **1989**, *243*, 1325.
- (2) Kohen, A.; Limbach, H. H. *Isotope Effects In Chemistry and Biology*; CRC Press: Boca Raton, FL, 2006.
- (3) *Quantum Tunnelling in Enzyme Catalyzed Reactions*; Allemann, R. K., Scrutton, N. S., Eds.; RSC: Cambridge, 2009.
- (4) Kamerlin, S. C. L.; Mavri, J.; Warshel, A. *FEBS Lett.* **2010**, *584*, 2759.
- (5) Hay, S.; Scrutton, N. S. *Nature Chem.* **2012**, *4*, 161.
- (6) Glowacki, D. R.; Harvey, J. N.; Mulholland, A. J. *Nature Chem.* **2012**, *4*, 169.
- (7) Truhlar, D. G. *J. Phys. Org. Chem.* **2010**, *23*, 660.
- (8) Kohen, A.; Cannio, R.; Bartolucci, S.; Klinman, J. P. *Nature* **1999**, *399*, 496.
- (9) Maglia, G.; Allemann, R. K. *J. Am. Chem. Soc.* **2003**, *125*, 13372.
- (10) Basran, J.; Harris, R. J.; Sutcliffe, M. J.; Scrutton, N. S. *J. Biol. Chem.* **2003**, *278*, 43973.
- (11) Isaacs, N. S. In *Isotope Effects in Organic Chemistry*; Buncl, E., Lee, C. C., Eds.; Elsevier, London: 1984; Vol. 6, p 67.
- (12) Northrop, D. B. *Phil. Trans. Royal Soc. B* **2006**, *361*, 1341.
- (13) Isaacs, N. S.; Javid, K.; Rannala, E. *Nature* **1977**, *268*, 372.
- (14) Northrop, D. B. *J. Am. Chem. Soc.* **1999**, *121*, 3521.
- (15) Hay, S.; Sutcliffe, M. J.; Scrutton, N. S. *Proc. Natl. Acad. Sci. U.S.A.* **2007**, *104*, 507.
- (16) Hay, S.; Scrutton, N. S. *Biochemistry* **2008**, *47*, 9880.
- (17) Pudney, C. R.; Hay, S.; Levy, C.; Pang, J. Y.; Sutcliffe, M. J.; Leys, D.; Scrutton, N. S. *J. Am. Chem. Soc.* **2009**, *131*, 17072.

- (18) Marchal, S.; Font, J.; Ribó, M.; Vilanova, M.; Phillips, R. S.; Lange, R.; Torrent, J. *Acc. Chem. Res.* **2009**, *42*, 778.
- (19) Northrop, D. B. *Biochim. Biophys. Acta* **2002**, *1595*, 71.
- (20) Hay, S.; Pudney, C. R.; Sutcliffe, M. J.; Scrutton, N. S. *J. Phys. Org. Chem.* **2010**, *23*, 696.
- (21) Masgrau, L.; Roujeinikova, A.; Johannissen, L. O.; Hothi, P.; Basran, J.; Ranaghan, K. E.; Mulholland, A. J.; Sutcliffe, M. J.; Scrutton, N. S.; Leys, D. *Science* **2006**, *312*, 237.
- (22) Johannissen, L. O.; Hay, S.; Scrutton, N. S.; Sutcliffe, M. J. *J. Phys. Chem. B* **2007**, *111*, 2631.
- (23) Hothi, P.; Hay, S.; Roujeinikova, A.; Sutcliffe, M. J.; Lee, M.; Leys, D.; Cullis, P. M.; Scrutton, N. S. *ChemBioChem* **2008**, *9*, 2839.
- (24) Hay, S.; Johannissen, L.; Sutcliffe, M. J.; Scrutton, N. S. *Biophys. J.* **2010**, *98*, 121.
- (25) Johannissen, L. O.; Scrutton, N. S.; Sutcliffe, M. J. *J. Royal. Soc. Interface* **2008**, *5*, S225.
- (26) Weber, G. *J. Phys. Chem.* **1993**, *97*, 7108.
- (27) Hay, S.; Pudney, C. R.; McGrory, T. A.; Pang, J. Y.; Sutcliffe, M. J.; Scrutton, N. S. *Angew. Chem., Int. Ed.* **2009**, *48*, 1452.
- (28) Hay, S.; Johannissen, L. O.; Sutcliffe, M. J.; Scrutton, N. S. *Biophys. J.* **2010**, *98*, 121.
- (29) Johannissen, L. O.; Scrutton, N. S.; Sutcliffe, M. J. *Angew. Chem., Int. Ed.* **2011**, *50*, 2129.
- (30) Caratzoulas, S.; Mincer, J. S.; Schwartz, S. D. *J. Am. Chem. Soc.* **2002**, *124*, 3270.
- (31) Roca, M.; Oliva, M.; Castillo, R.; Moliner, V.; Tunon, I. *Chem.—Eur. J.* **2010**, *16*, 11399.
- (32) Agarwal, P. K.; Billeter, S. R.; Rajagopalan, P. T. R.; Benkovic, S. J.; Hammes-Schiffer, S. *Proc. Natl. Acad. Sci. U.S.A.* **2002**, *99*, 2794.
- (33) Hatcher, E.; Soudackov, A. V.; Hammes-Schiffer, S. *J. Am. Chem. Soc.* **2007**, *129*, 187.
- (34) Antoniou, D.; Schwartz, S. D. *Proc. Natl. Acad. Sci. U.S.A.* **1997**, *94*, 12360.
- (35) Kuznetsov, A. M.; Ulstrup, J. *Can. J. Chem.* **1999**, *77*, 1085.
- (36) Knapp, M. J.; Rickert, K.; Klinman, J. P. *J. Am. Chem. Soc.* **2002**, *124*, 3865.
- (37) Soudackov, A.; Hatcher, E.; Hammes-Schiffer, S. Quantum and dynamical effects of proton donor-acceptor vibrational motion in nonadiabatic proton-coupled electron transfer reactions *J. Chem. Phys.* **2005**, *122*.
- (38) Meyer, M. P.; Klinman, J. P. *Chem. Phys.* **2005**, *319*, 283.
- (39) Hatcher, E.; Soudackov, A. V.; Hammes-Schiffer, S. *J. Am. Chem. Soc.* **2004**, *126*, 5763.
- (40) Hothi, P.; Khadra, K. A.; Combe, J. P.; Leys, D.; Scrutton, N. S. *FEBS J.* **2005**, *272*, 5894.
- (41) Brooks, B. R.; et al. *J. Comput. Chem.* **2009**, *30*, 1545.
- (42) MacKerell, A. D.; et al. *J. Phys. Chem. B* **1998**, *102*, 3586.
- (43) Antoniou, D.; Basner, J.; Nunez, S.; Schwartz, S. D. *Chem. Rev.* **2006**, *106*, 3170.